

# High-Resolution In Vivo Imaging of the RPE Mosaic in Eyes with Retinal Disease

Austin Roorda,<sup>1</sup> Yuhua Zhang,<sup>1</sup> and Jacque L. Duncan<sup>2</sup>

**PURPOSE.** To use high-resolution and contrast imaging techniques to reveal microscopic retinal structures, including individual retinal pigment epithelial (RPE) cells, in human eyes with inherited retinal disease.

**METHODS.** Adaptive optics scanning laser ophthalmoscopy (AOSLO) was used to image the macular region in patients with retinal degenerative diseases, including two patients with cone-rod dystrophy and one with bilateral progressive maculopathy. Images were processed, and the microscopic details were analyzed. Fundus-related microperimetry was used to assess visual function within retinal regions where no cones were visible.

**RESULTS.** In addition to patches of intact cone photoreceptors, AOSLO images revealed mosaics of RPE cells in regions where it appeared that cones were missing. In cone-rod dystrophy (CRD), the RPE cells were visualized in an annular region surrounding a cone-preserved central area. RPE cell shape, size, and distribution compared well with measurements from the literature. Fundus-related microperimetry results indicated scotomas that corresponded to the locations where RPE cells were visible.

**CONCLUSIONS.** For the first time, the mosaic of RPE cells has been directly visualized by AOSLO. Patients with hereditary retinal degenerations causing cone loss in the macula allowed visualization of RPE cells in areas where cones were missing. Regions with visible RPE cells demonstrated loss of visual function measured using microperimetry. (*Invest Ophthalmol Vis Sci.* 2007;48:2297-2303) DOI:10.1167/iovs.06-1450

The retinal pigment epithelium (RPE) is a single layer of cells in the eye, located adjacent and posterior to the photoreceptor layer. The RPE has many important roles in vision, playing an active role in the visual cycle, absorbing stray light, forming a blood-retinal barrier between the retina and choroid, and maintaining the cones, including nourishment and

phagocytosis of the cone and rod outer segments.<sup>1-4</sup> Dysfunction of the RPE layer, particularly relating to its role in the visual cycle, is implicated in many disease processes, including cone-rod dystrophy,<sup>5-7</sup> retinitis pigmentosa,<sup>5,8-11</sup> age-related macular degeneration,<sup>12</sup> Best macular dystrophy,<sup>13</sup> and Stargardt disease.<sup>14</sup>

The extent of current knowledge of RPE morphology and structure in normal and diseased eyes has been obtained from postmortem tissue,<sup>15-18</sup> as direct visualization of the RPE in living eyes has been very difficult. Given that (1) their size is larger than 10  $\mu\text{m}$  in diameter and (2) they are a relatively strong source of scatter in the retina (based on OCT images),<sup>19,20</sup> they should be visible in a well-focused retinal image. But several factors conspire to limit their visibility. First, although a lot of scattered light from the fundus comes from the RPE, it is masked by the light that comes from the overlying photoreceptor mosaic, which is also a strong scattering layer.<sup>20</sup> Second, even if the light from the RPE were to reach the camera directly, the intrinsic contrast of the cells is limited. In fact, the mechanisms by which direct, scattered light emerges from the RPE layer to allow for its visualization in the living eye is unknown. Finally, although the optics of an eye that is well-corrected for defocus and astigmatism is sufficient to resolve small features,<sup>21</sup> their contrast is still limited at the 10- $\mu\text{m}$  scale and so optical blur from aberrations imposes the final limit on the visibility of the RPE layer.

Recently, major advances in the visualization of the RPE in living primates was achieved with high-magnification, high-resolution autofluorescence in an adaptive optics scanning laser ophthalmoscopy (AOSLO).<sup>22</sup> These results are the first demonstration that when proper contrast mechanisms and imaging modalities are used, the mosaic of RPE cells can be revealed.

In this study, we also used an AOSLO,<sup>23</sup> but with direct confocal imaging, to image directly the array of RPE cells in several patients with retinal disease. The RPE cells were directly visible with infrared light imaging in regions where the cones were presumed to be absent.

## METHODS

This research adhered to the tenets of the World Medical Association Declaration of Helsinki. Informed consent was obtained from the subjects after we explained the nature and possible complications of the study. The experiments were approved by the Committee for the Protection of Human Subjects at the Berkeley and San Francisco campuses of the University of California. Clinical information, AOSLO cone images, and quantitative cone analysis from patients 1 and 3 have been reported elsewhere<sup>24</sup> (Duncan JL et al. *IOVS* 2006;47:ARVO E-Abstract 5667).

All subjects underwent a complete eye examination by an ophthalmologist (JLD), including measurement of best-corrected visual acuity (BCVA) with a Snellen chart. Acuity equal to or better than 20/20 were recorded as 20/20. Visual acuity was reported as the quotient of the Snellen acuity (i.e., 20/20 = 1.0). Color fundus photographs taken by outside ophthalmologists in the past were used when available, and in one subject digital color fundus photographs and a fluorescein angiogram were obtained (FF4 System; Carl Zeiss Meditec, Inc., Dub-

---

From the <sup>1</sup>UC Berkeley School of Optometry, University of California, Berkeley, Berkeley, California; and the <sup>2</sup>Department of Ophthalmology, University of California, San Francisco, San Francisco, California.

Supported by National Institutes of Health Bioengineering Research Partnership Grant EY014375 (AR); National Science Foundation Science and Technology Center for Adaptive Optics, managed by the University of California at Santa Cruz under cooperative agreement AST-9876783 (AR); the Foundation Fighting Blindness (JLD, AR); Career Development Awards from Research to Prevent Blindness and the Foundation Fighting Blindness (JLD); National Eye Institute Grant EY00415 (JLD); That Man May See, Inc. (JLD); and The Bernard A. Newcomb Macular Degeneration Fund (JLD).

Submitted for publication December 7, 2006; revised January 16, 2007; accepted March 15, 2007.

Disclosure: **A. Roorda** (P); **Y. Zhang**, None; **J.L. Duncan**, None  
The publication costs of this article were defrayed in part by page charge payment. This article must therefore be marked "advertisement" in accordance with 18 U.S.C. §1734 solely to indicate this fact.

Corresponding author: Austin Roorda, University of California, Berkeley, School of Optometry, Room 485, Minor Hall, Berkeley, CA 94720-2020; aroorda@berkeley.edu.

lin, CA with software by Ophthalmic Imaging Systems, Inc., Sacramento, CA). Optical coherence tomography (OCT) images were obtained using the OCT system software (Stratus OCT 4.0.2; Carl Zeiss Meditec, Inc.) to determine retinal thickness with the fast macular protocol and 6-mm horizontal and vertical lines centered on the anatomic fovea. Retinal thickness was measured with calipers to mark the vitread surface of the foveal dip and the first highly reflective band sclerad to the vitread surface on a 6-mm horizontal scan. Pupils were dilated with 1% tropicamide and 2.5% phenylephrine before full-field electroretinography (ERG), which was performed after 45 minutes of dark adaptation by using a Burian-Allen contact lens electrode, according to standards specified by the International Society for Clinical Electrophysiology and Vision (ISCEV).<sup>25</sup> Multifocal (mf)ERG testing was performed in the light-adapted state (VERIS 5.1.10X, Electro-Diagnostic Imaging, Inc., Redwood City, CA) with a Burian-Allen contact lens electrode (Hansen Ophthalmic Development Laboratory, Iowa City, IA), according to the ISCEV standards.<sup>26</sup> Responses were recorded using 16 30-second sequences in each eye. The stimulus consisted of 103 elements covering the central 40° diameter of the visual field, the flash intensity was 200 cd/m<sup>2</sup>, the intensity of dark frames was less than 4 cd/m<sup>2</sup>, and the average luminance was 100 cd/m<sup>2</sup>. Fixation was monitored with an infrared eye camera. The signal was amplified 100,000 times, and the bandwidth was set at 10 to 100 Hz. A single iteration of 17% spatial averaging was performed using the VERIS software. Response amplitudes of the first-order waveform were measured from N1 to P1 and the latency of the P1 response was reported.

### Genetic Testing

Patient 3 was studied on a research basis for X-linked mutations at the University of Michigan. Genetic tests were also performed on a fee-for-service basis performed by CLIA-certified laboratories (The University of Iowa Diagnostic Laboratories and Carver Laboratory for Molecular Diagnosis, Iowa City, IA, and The University of Michigan Ophthalmic Molecular Diagnostic Laboratory, Ann Arbor, MI). Seven to 9 mL of whole blood was obtained for molecular analysis of RDS and ABCA4 in patient 2. Blood from patient 1 was sent for molecular analysis of the CRX and ABCA4 genes.

### Imaging

To image the RPE cells, we used our latest generation of the AOSLO.<sup>27</sup> Adaptive optics describes a set of methods for measuring and compensating for the aberrations of individual eyes.<sup>28</sup> Our laboratory has integrated adaptive optics into an SLO and, by removing the blur from the eye's aberrations, have shown real-time microscopic views of living retina, including direct visualization of cone photoreceptors and the flow of single white blood cells.<sup>29</sup> The AOSLO is a confocal device, giving it high contrast in the image plane as well as the ability to perform optical slicing of tissue.<sup>30</sup> Recently, we have completed a second-generation AOSLO. This device is more compact, uses a low coherence, infrared light source to reduce speckle artifacts and has an overall improved electronic and system design. A series of videos, each spanning a 1.2° × 1.2° field, were taken in a grid of retinal locations of three patients. Adaptive optics was used to reduce blur from aberrations in each video at each retinal location.

### Image Analysis

Each individual video was processed to generate a high signal-to-noise static frame. The processing included three steps: correction of distortion in frames caused by the sinusoidal velocity profile of the scanning mirror, removal of image frame distortion caused by eye movements,<sup>31,32</sup> and frame averaging. No further processing or nonlinear filtering was performed on the images. The series of static frames were stitched together into a larger image with image management software (Photoshop software; Adobe Systems Inc., Mountain View, CA). Unambiguous matches of microscopic features from frame to frame were used to guide the matches.

Presumed RPE cells in the mosaic were identified by hand with custom software. The RPE cell locations were analyzed with a measurement called the density recovery profile (DRP), which is a method devised by Rodieck<sup>33</sup> to quantify the spatial arrangement of cells.<sup>34</sup> The DRP plots the average histogram of density of all cells surrounding each cell in the mosaic as a function of distance from the central cone. Specific features in the DRP provide useful information on the packing structure. First, if the structure is regular (crystalline), then there will be oscillations in the DRP corresponding to the nearest, secondary, and tertiary neighbors. The distance to the first peak in the DRP indicates the nearest neighbor distance, the cell size and the cell spacing (assuming a regular close-packed mosaic of cells).

### Functional Testing: Microperimetry

Fundus-related microperimetry was performed in one of the patients by using infrared illumination to image the retina and track retinal landmarks specified at the start of the test (MPI; Nidek Technologies America, Inc., Greensboro, NC). The central 8° visual field was tested with a Goldmann III stimulus of 200-ms duration with a 4-2 threshold strategy. Subjects were instructed to fixate on the center of four crosses, each 2° in size at an eccentricity of 5°, and fixation was monitored for both locations with respect to the fovea, judged by anatomic landmarks and stability. Numeric microperimetry results were exported, and results were overlaid with AOSLO images by using a custom-written program (written in MatLab; The MathWorks, Natick, MA).

### Functional Testing: AOSLO Microperimetry

With an SLO, it is possible to project stimuli directly onto the retina by modulating the laser beam during the raster scan.<sup>35</sup> Given the resolution of the AO-corrected image and the fact that the same laser is used to project the stimuli, we can exactly identify the retinal location of the projected stimuli to within a single cone photoreceptor in the AOSLO.<sup>36</sup> We used this feature to identify the location of the fovea of the patient who underwent the microperimetry tests. The foveal location that was identified from this test was used to ensure correct alignment between the microperimetry plots and the AOSLO images.

## RESULTS

### Case 1: Cone-Rod Dystrophy

Patient 1 was a 41-year-old man with simplex CRD whose vision was reduced to 20/80 OD and 20/200 OS. OCT (Carl Zeiss Meditec, Inc.) images showed significant thinning in the macula and an absence of the classic laminar appearance of the photoreceptor layer. The composite AOSLO image from the right eye of patient 1 is shown in Figure 1. In this image, sparse cones with increased cone spacing are present near his preferred retinal locus. Beyond the region where cones are seen, a region of hexagonal cells is present, corresponding to the region of preserved RPE seen on fundus photography. This image shows the largest number of visible RPE cells that we have observed to date. The marks in the image at the top right show the subset of RPE cells with positions manually identified for analysis. The bottom right image shows the cone-preserved region (central) and the visible RPE region (irregular annulus). The presence of cones in the cone-preserved region was confirmed by asking the patient to fixate on a stimulus that was projected directly on the retina by the AOSLO. When presented with a salient target, the patient's fixation was very stable, and visual observation of the fundus in the AOSLO videos suggested that fixation was no worse than that of a healthy fixating eye. The mosaic of cones is visible only in the top right corner of the cone-preserved region. Cone spacing in this region was about twice that of a normal healthy eye<sup>24</sup> (Duncan JL et al. *IOVS* 2006;47:ARVO E-Abstract 5667) result-

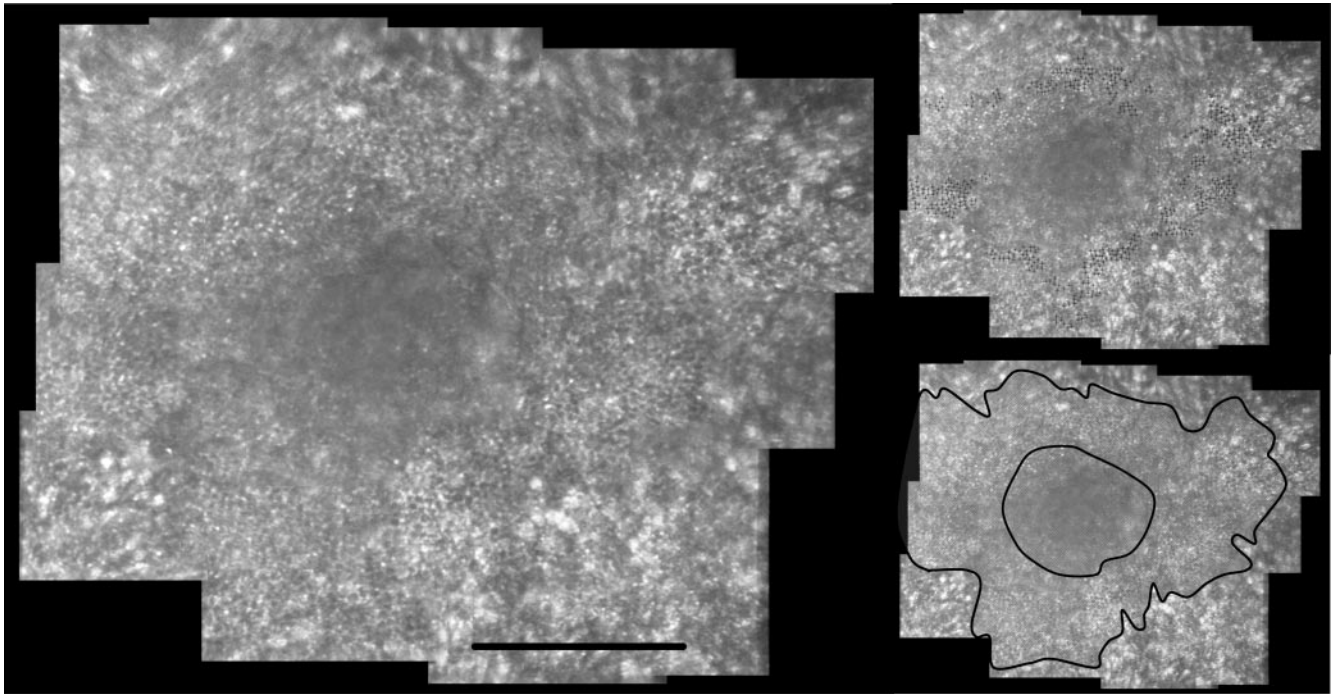


**FIGURE 1.** Composite image of a patient with cone-rod dystrophy. The complete image (*left*) spans approximately  $4.25 \times 3.3^\circ$  (scale bar is  $1^\circ$ ). *Top right*: locations of the RPE cells that were used for the spacing analysis. *Bottom right*: cone-preserved region (central zone) and the extent of the irregular annular zone where the RPE cells were visualized. The annular zone of RPE cells lie within the bull's-eye lesion that can be seen in a conventional fundus photograph.

ing in approximately a fourfold drop in density. Similar observations of low cone density in patients with CRD were also reported by Wolfing et al.<sup>37</sup> and Choi et al.<sup>38</sup>

**RPE Cell Size and Density.** Figure 1 shows the subset of RPE cells that were manually selected for analysis (top right). Not all cells have to be identified to complete a spacing analysis

by using the DRP method, and so only the most visible cells were selected. The results of the DRP analysis are plotted in Figure 2. The oscillatory nature of the DRP indicates that the identified cells had a regular or crystalline packing structure, consistent with RPE cells.<sup>18</sup> The distance to the first peak was at 3.04 minutes of arc, or approximately  $15.2 \mu\text{m}$ .

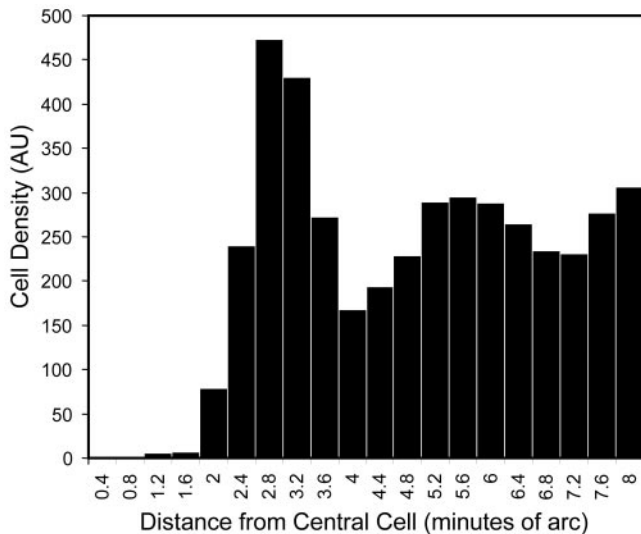


**FIGURE 2.** Density recovery profile for the subset of RPE cells identified in Figure 1. The nearest neighbor cells peak in density at 3.04 minutes of arc, which corresponds to an approximate distance of  $15.20 \mu\text{m}$  (assuming that  $1^\circ$  of visual angle corresponds to a  $300 \mu\text{m}$  span on the retina). The average distance of the measured RPE cells from the foveal center is approximately  $1^\circ$ . The regularity of the packing and the consistency of cell size are clear from the oscillatory nature of the DRP.

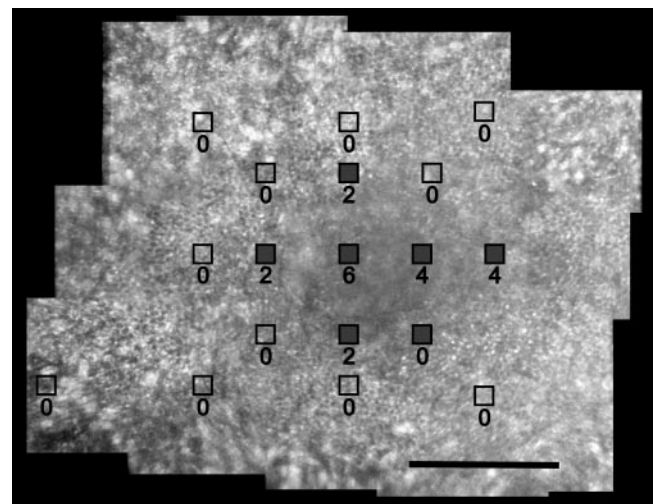


**FIGURE 3.** Microperimetry (MP; Nidek, Technologies America, Inc., Greensboro, NC) results superimposed on the AOSLO image. The numbers indicate the attenuation scale in decibels; 20-dB sensitivity is expected from normal subjects representing a differential luminance of  $1.27 \text{ cd/m}^2$ . Absolute scotomas, indicated by empty squares and labeled 0, correspond to regions with visible RPE cells as well as regions with RPE atrophy (hyperreflective regions). Measurable visual function with reduced sensitivity is retained in the central region, where some cones are preserved, albeit at lower density than in a normal eye. The scale bar represents  $1^\circ$  of visual field, or approximately  $300 \mu\text{m}$ .

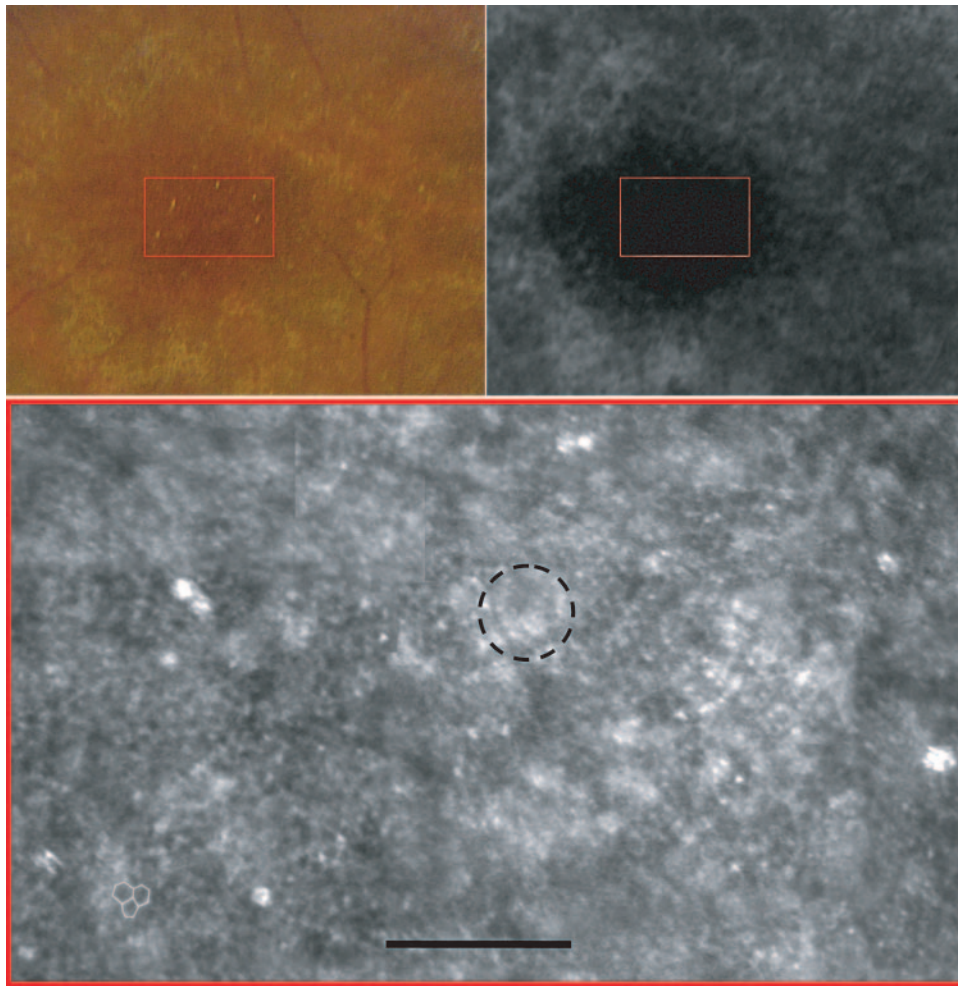


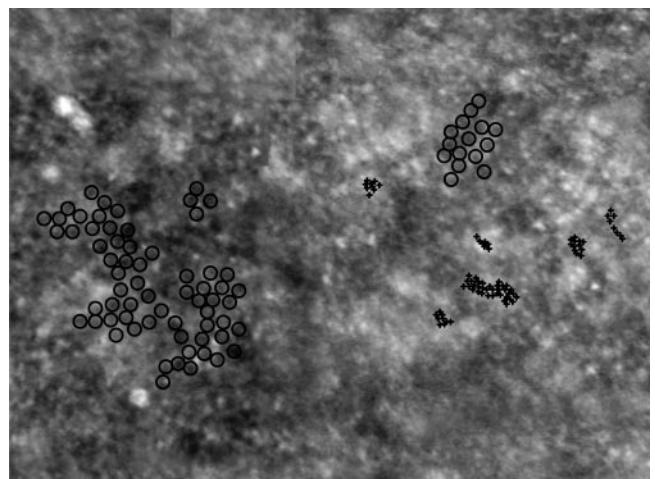
**FIGURE 4.** Case 2: fundus photograph (*top left*), fluorescein angiogram at 48 seconds after injection (*top right*) and AOSLO image (*bottom*). The fundus photograph shows RPE mottling surrounding a central region of preserved RPE where focal yellow spots are present. On fluorescein angiography, the region of RPE mottling demonstrated a window defect consistent with RPE loss, with central hypofluorescence due to blocking centrally in the region with preserved RPE cells. The AOSLO image revealed a patchy foveal cone mosaic with increased cone spacing. The preferred retinal locus is indicated by the *dashed circle* in the image, but fixation was unstable compared with normal. RPE cells filled the remaining area. To orient the reader, three RPE cells in the *bottom left corner* have been outlined. The brighter RPE cells in the AOSLO image match the *yellow spots* in the fundus photograph. The average size of the RPE cells in this region is 14.85  $\mu\text{m}$ . Scale bar, 0.25° or  $\sim 75 \mu\text{m}$ .

**Functional Imaging Results.** Nidek MP1 microperimetry revealed a small central region with reduced vision surrounded by an annular scotoma. Fixation was reported from the MP1 as stable, remaining within 2° of the target 97% of the time and within 4° 100% of the test session. Figure 3 shows an overlay of the microperimetry results in an AOSLO image. The alignment between the microperimetry maps and the image was guided by the foveal identification method, as described in the Methods section.

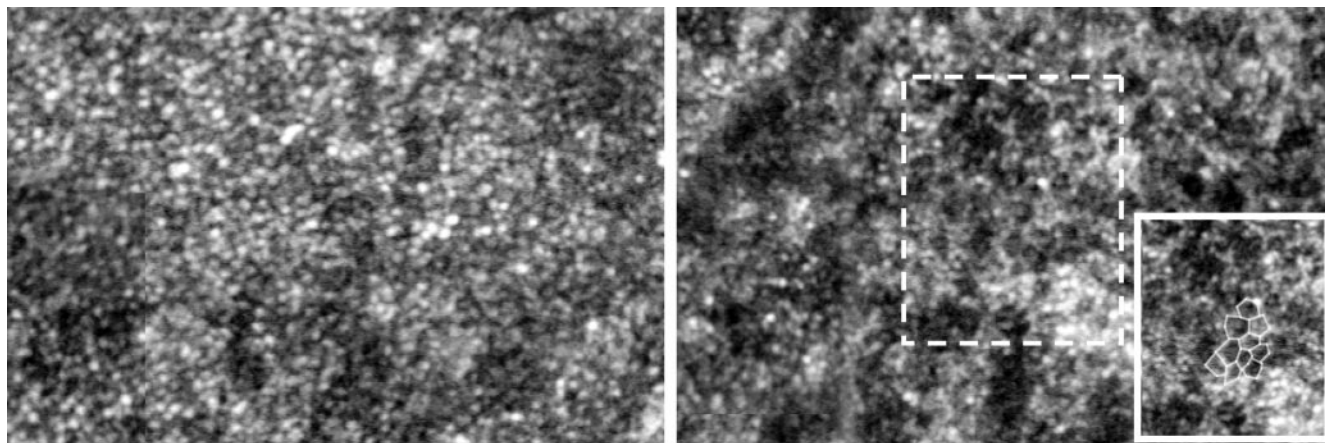
### Case 2: Bilateral Progressive Maculopathy

Figure 4 shows an image of a 49-year-old patient with bilateral progressive central vision loss. She reported having had nyctalopia for the past 8 years, with subsequent development of photophobia and reduced color vision. Best corrected visual acuity was 20/100 OD and 20/70 OS. Full-field ERG testing revealed normal rod- and cone-mediated retinal function, but slightly delayed mixed scotopic a- and b-waves, and multifocal ERG testing demonstrated reduced responses with delayed timing throughout the central 30° in each eye. Molecular analysis revealed no disease-causing mutations in the genes for ABCA4 or peripherin/RDS. OCT (Carl Zeiss Meditec, Inc.) images showed significant thinning in the macula and an absence of the classic laminar appearance of the photoreceptor layer. Fundus photographs and fluorescein angiography both suggest the presence of RPE cells in the foveal region, surrounded by an area of RPE atrophy. The AOSLO image showed a very patchy cone mosaic, and RPE cells could be seen over much of the macular region but, unlike in the CRD case, they did not

form an annular pattern. The lighter areas are presumed to be cones. In some regions the cone mosaic could be seen but the cones did not appear with the same contrast and were not contiguous as in a normal, healthy eye. Figure 5 shows the same region as Figure 4 with the RPE cells and cones indicated.



**FIGURE 5.** The subset of visible RPE cells that were selected for the spacing analysis. *Circles*: RPE; *crosses*: a selection of unambiguous cones, which tend to lie in the lighter regions of the image in this case.



**FIGURE 6.** *Left:* retina of a patient with early-stage CRD at approximately  $1^\circ$  from the fovea. The cone spacing is greater than normal but the mosaic is contiguous at this location. *Right:* a region  $\sim 2.5^\circ$  from the fovea. The RPE cells are present between sparse cones (*insets:* RPE outlines). The RPE cells at this location are 2.97 minutes in size or approximately  $14.85 \mu\text{m}$ . Scale bar,  $0.5^\circ$  or  $\sim 150 \mu\text{m}$ .

The bright spots in the fundus photographs matched those in the AOSLO image and appear to be hyperreflective RPE cells.

### Case 3: Early Stage Cone-Rod Dystrophy

This 32-year-old man with a family history of X-linked CRD demonstrated reduced cone function on full-field and mfERG testing, despite retaining best-corrected visual acuity of 20/20. OCT (Carl Zeiss Meditec, Inc.) images showed significant thinning in the macula with moderate lamination due to a thinned but present photoreceptor layer. This patient had a deletion in exon ORF (open reading frame) 15 of *RPGR*, resulting in the frameshift mutation Glu481GlyfsX492. This novel mutation is at the 3' end of ORF15, where other mutations in patients with XLCRD have been reported.<sup>39</sup> More information about this patient can be found in another paper.<sup>24</sup>

In this case, photoreceptors were visualized across most of the macula although with increased spacing, or decreased density, compared to normal.<sup>24</sup> However, the cone mosaic appeared patchy and nonuniform and RPE cell structure was visible in some small regions. We identified the cells in the

regions where we were most confident that they could be seen and measured the spacing. One such region is shown in the Figure 6, right. For comparison, the Figure 6, left, shows a region for the same subject where a contiguous cone mosaic is resolved. It is not known whether there were functioning cones present in the region where the mosaic of RPE cells was visible in the right image.

The same patient was imaged 7 months later with the same system. Figure 7 shows the same regions and that the RPE cells are resolved on both visits.

### DISCUSSION

RPE cells have been difficult to resolve in living eyes. To date, there are no reports of visualization of these cells through direct imaging *in vivo*. A recent publication by Gray et al.<sup>22</sup> shows images of RPE cells obtained with AOSLO autofluorescence imaging in an anesthetized monkey eye.

Why are the RPE cells so difficult to see, especially when they are purported to be one of the major sources of scattering

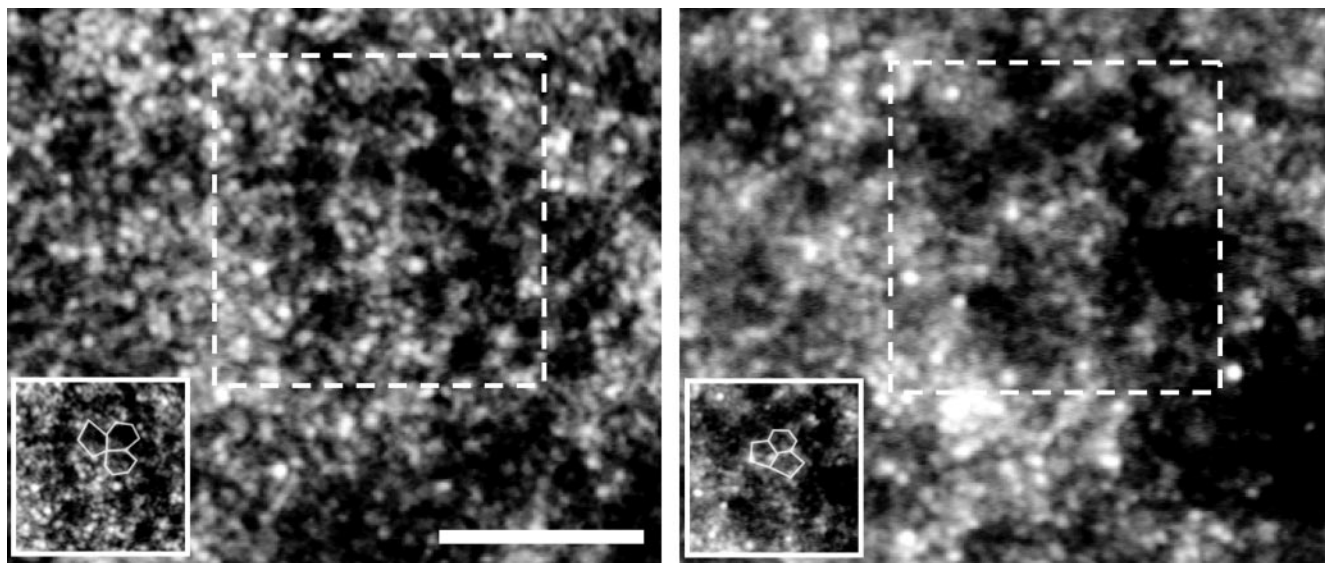


**FIGURE 7.** Images of the same retinal region taken 7 months apart. Despite differences in the appearance between the images, several RPE cells are resolved (outlined in *bottom left insets*). The average size of the RPE cells in this region is  $14.85 \mu\text{m}$ . Scale bar,  $0.25^\circ$  or  $\sim 75 \mu\text{m}$ .

in OCT images?<sup>20</sup> The reason is that, in a normal eye, the RPE lies just posterior to the photoreceptors which are also strong scattering sources. Although the AOSLO is confocal and has the ability to optically section the retinal tissue,<sup>30</sup> its axial resolution is modest compared with OCT, and so scattered light from the photoreceptors and the RPE is contained in the same axial section. Furthermore, the nature of the scattered light from the RPE layer is likely to be affected by the presence of the photoreceptors, and so even if scattered light from RPE is collected by the detector, the structure of the cell mosaic may not be apparent. In conditions in which the photoreceptor layer is compromised or missing and the scattered light from the photoreceptors is no longer present, the true structure of the RPE is revealed. The high-contrast images of the AOSLO instrument enhance the contrast of RPE cell structure to the extent that RPE cells can be directly observed. Autofluorescence from lipofuscin, in contrast, is not wave-guided,<sup>40</sup> and so, even in a retina with intact photoreceptors, RPE structure can be visualized using a good imaging system.<sup>22</sup>

Visualization of RPE cells using direct backscattered light provides insight into the stages of disease progression in patients with retinal degenerations. Conventional clinical ophthalmoscopes cannot distinguish between regions with or without intact photoreceptors, as long as the RPE is present. For example, the retinal structure within a macular bull's eye lesion of RPE atrophy often appears uniform in a clinical examination. However, with a combination of adaptive optics imaging and fundus-related microperimetry we find very important changes within the center of the bull's eye. The images suggest that RPE cells remain, even after photoreceptors are gone. Regions with no visible photoreceptors correspond with absolute scotomas, and regions where photoreceptors remain have increased spacing (reduced density) and reduced visual function. Over time, we postulate that the RPE cells will become atrophic and appear as clinically visible regions of RPE atrophy, but longitudinal measures are needed to test this hypothesis.

Fundus autofluorescence has been used as a measure of lipofuscin deposits in the RPE cells in patients with retinal degenerations, including age-related macular degeneration,<sup>41</sup> retinitis pigmentosa,<sup>42,43</sup> Best macular dystrophy,<sup>44</sup> and Stargardt disease.<sup>45</sup> Although the present study does not include autofluorescence imaging, AOSLO images may provide a novel modality for imaging RPE cell structure in patients with retinal degenerations. An advantage to the use of AOSLO to image RPE cells is the infrared light source used, because shorter wavelengths of light such as those traditionally used to image autofluorescence have been associated with damage in animal models of retinal degeneration<sup>46,47</sup> and with RPE cells in culture fed a component of lipofuscin, A2-E.<sup>48</sup>

The size of the RPE cells observed in the present study is consistent with that observed in the literature. Gao and Hollyfield<sup>15</sup> report RPE cell center-to-center spacing ranging from 12.45  $\mu\text{m}$  at the fovea to 13.87  $\mu\text{m}$  at 120  $\mu\text{m}$  from the foveal center. Watzke et al.<sup>18</sup> report center-to-center spacing of 14  $\mu\text{m}$  in a region within 250  $\mu\text{m}$  of the foveal center. Dorey et al.<sup>16</sup> report the smallest RPE cell sizes of 10.13  $\mu\text{m}$ , but these values were inferred from histologic cross-sections. All these reports are from excised human ocular tissue. Our measurements range from 14.85 to 15.2  $\mu\text{m}$  in regions ranging in eccentricity from 100 to 750  $\mu\text{m}$  from the foveal center.

Further evidence that these are indeed RPE cells is their regular packing structure. Primary, secondary, and tertiary oscillations of the DRP indicate that the cells are closely packed, and a honeycomb appearance due to the hexagonal packing structure is readily observed in the images. Similar hexagonal packing is observed in en face microscopy imaging.<sup>18</sup>

## CONCLUSION

This is the first report showing direct visualization of the RPE cells in a human eye. The visibility of RPE cells using direct backscattered light identifies regions where photoreceptors no longer scatter or wave-guide light and are no longer functioning. Visualizing the RPE and other retinal structures on this scale may be useful in diagnosing or monitoring the progression of retinal disease. This work represents a first step toward imaging the structural and basic functional properties in cases of retinal degeneration in which RPE cells can be seen. Further work is needed to identify the sources within the RPE cell that scatter light. In addition, we plan to perform additional studies using AOSLO to gain a better definition of the anatomic properties of the RPE cells visualized, using filters to image autofluorescence as a measure of lipofuscin content. We also plan to use AOSLO to deliver stimuli with high resolution to assess visual function in regions where RPE cells are seen. Finally, we plan to observe patients in whom RPE cells are visible longitudinally, to determine whether the RPE cells are visible during a stage in progressive degeneration or whether these visible RPE cells represent a unique phenotype for a subset of retinal diseases.

## References

1. Thumann G, Hinton DR. Cell biology of the retinal pigment epithelium. In: Ogden TE, Hinton DR, eds. *Retina: Basic Science and Inherited Retinal Disease*. Vol 1. St. Louis: CV Mosby; 2001;104-121.
2. Bok D. The retinal pigment epithelium: a versatile partner in vision. *J Cell Sci Suppl*. 1993;17:189-195.
3. Bringmann A, Reichenbach A, Weidemann P. Pathomechanisms of cystoid macular edema. *Ophthalmic Res*. 2004;36:241-249.
4. Marmor MF. Mechanisms of fluid accumulation in retinal edema. *Doc Ophthalmol*. 1999;97:239-249.
5. Gu SM, Thompson DA, Srikumari CR, et al. Mutations in RPE65 cause autosomal recessive childhood-onset severe retinal dystrophy. *Nat Genet*. 1997;17:194-197.
6. Maugeri A, Klevering BJ, Rohrschneider K, et al. Mutations in the ABCA4 (ABCR) gene are the major cause of autosomal recessive cone-rod dystrophy. *Am J Hum Genet*. 2000;67:960-966.
7. Ducrocq D, Rozet JM, Gerber S, et al. The ABCA4 gene in autosomal recessive cone-rod dystrophies. *Am J Hum Genet*. 2002;71:1480-1482.
8. Hayward C, Shu X, Cideciyan AV, et al. Mutation in a short-chain collagen gene, CTRP5, results in extracellular deposit formation in late-onset retinal degeneration: a genetic model for age-related macular degeneration. *Hum Mol Genet*. 2003;12:2657-2667.
9. Gal A, Li Y, Thompson DA, et al. Mutations in MERTK, the human orthologue of the RCS rat retinal dystrophy gene, cause retinitis pigmentosa. *Nat Genet*. 2000;26:270-271.
10. Thompson DA, Li Y, McHenry CL, et al. Mutations in the gene encoding lecithin retinol acyltransferase are associated with early-onset severe retinal dystrophy. *Nat Genet*. 2001;28:123-124.
11. Maw MA, Kennedy B, Knight A, et al. Mutation of the gene encoding cellular retinaldehyde-binding protein in autosomal recessive retinitis pigmentosa. *Nat Genet*. 1997;17:198-200.
12. Zarbin MA. Current concepts in the pathogenesis of age-related macular degeneration. *Arch Ophthalmol*. 2004;122:598-614.
13. Petrukhin K, Koisti MJ, Bakall B, et al. Identification of the gene responsible for Best macular dystrophy. *Nat Genet*. 1998;19:241-247.
14. Weng J, Mata NL, Azarian SM, et al. Insights into the function of Rim protein in photoreceptors and etiology of Stargardt's disease from the phenotype in abcr knockout mice. *Cell*. 1999;98:13-23.
15. Gao H, Hollyfield JG. Aging of the human retina: differential loss of neurons and retinal pigment epithelial cells. *Invest Ophthalmol Vis Sci*. 1992;33:1-17.
16. Dorey CK, Wu G, Ebenstein D, Garsd A, Weiter JJ. Cell loss in the aging retina: relationship to lipofuscin accumulation and macular

- degeneration. *Invest Ophthalmol mol Vis Sci.* 1989;30:1691-1699.
17. Panda-Jonas S, Jonas JB, Jakobczyk-Zmija M. Retinal pigment epithelial cell count, distribution, and correlations in normal human eyes. *Am J Ophthalmol.* 1996;121:181-189.
  18. Watzke RC, Soldevilla JD, Trune DR. Morphometric analysis of human retinal pigment epithelium: correlation with age and location. *Curr Eye Res.* 1993;12:133-142.
  19. Drexler W, Morgner U, Ghanta RK, et al. Ultrahigh-resolution ophthalmic optical coherence tomography. *Nat Med.* 2001;7:502-507.
  20. Zhang Y, Rha J, Jonnal RS, Miller DT. Adaptive optics parallel spectral domain optical coherence tomography for imaging the living retina. *Opt Express.* 2005;13:4792-4811.
  21. Miller DT, Williams DR, Morris GM, Liang J. Images of cone photoreceptors in the living human eye. *Vision Res.* 1996;36:1067-1079.
  22. Gray DC, Merigan W, Wolfing JI, et al. In vivo fluorescence imaging of primate retinal ganglion cells and retinal pigment epithelium cells. *Opt Express.* 2006;14:7144-7158.
  23. Roorda A, Romero-Borja F, Donnelly WJ, et al. Adaptive optics scanning laser ophthalmoscopy. *Opt Express.* 2002;10:405-412.
  24. Duncan JL, Zhang Y, Gandhi J, et al. High resolution imaging of foveal cones in patients with inherited retinal degenerations using adaptive optics. *Invest Ophthalmol Vis Sci.* In press.
  25. Marmor MF, Holder GE, Seeliger MW, Yamamoto S. Standard for clinical electroretinography (2004 update). *Doc Ophthalmol.* 2004;108:107-114.
  26. Marmor MF, Hood DC, Keating D, et al. Guidelines for basic multifocal electroretinography (mfERG). *Doc Ophthalmol.* 2003;106:105-115.
  27. Zhang Y, Poonja S, Roorda A. MEMS-based adaptive optics scanning laser ophthalmoscope. *Opt Letts.* 2006;31:1268-1270.
  28. Liang J, Williams DR, Miller D. Supernormal vision and high-resolution retinal imaging through adaptive optics. *J Opt Soc Am A.* 1997;14:2884-2892.
  29. Martin JA, Roorda A. Direct and noninvasive assessment of parafoveal capillary leukocyte velocity. *Ophthalmology.* 2005;112:2219-2224.
  30. Romero-Borja F, Venkateswaran K, Roorda A, Hebert TJ. Optical slicing of human retinal tissue *in vivo* with the adaptive optics scanning laser ophthalmoscope. *Appl Opt.* 2005;44:4032-4040.
  31. Vogel CR, Arathorn DW, Roorda A, Parker A. Retinal motion estimation and image dewarping in adaptive optics scanning laser ophthalmoscopy. *Opt Express.* 2006;14:487-497.
  32. Stevenson SB, Roorda A. Correcting for miniature eye movements in high resolution scanning laser ophthalmoscopy. In: Manns F, Soderberg P, Ho A, eds. *Ophthalmic Technologies XI.* Bellingham, WA: SPIE; 2005;145-151.
  33. Rodieck RW. The density recovery profile: a method for the analysis of points in the plane applicable to retinal studies. *Vis Neurosci.* 1991;6:95-111.
  34. Roorda A, Metha AB, Lennie P, Williams DR. Packing arrangement of the three cone classes in primate retina. *Vision Res.* 2001;41:1291-1306.
  35. Timberlake GT, Mainster MA, Webb RH, Hughes GW, Trempe CL. Retinal localization of scotomata by scanning laser ophthalmoscopy. *Invest Ophthalmol Vis Sci.* 1982;22:91-97.
  36. Poonja S, Patel S, Henry L, Roorda A. Dynamic visual stimulus presentation in an adaptive optics scanning laser ophthalmoscope. *J Refract Surg.* 2005;21:S575-S580.
  37. Wolfing JI, Chung M, Carroll J, Roorda A, Williams DR. High-resolution retinal imaging of cone-rod dystrophy. *Ophthalmology.* 2006;113:1014-1019.
  38. Choi SS, Doble N, Hardy JL, et al. In vivo imaging of the photoreceptor mosaic in retinal dystrophies and correlations with visual function. *Invest Ophthalmol Vis Sci.* 2006;47:2080-2092.
  39. Demirci FY, Rigatti BW, Wen G, et al. X-linked cone-rod dystrophy (locus COD1): identification of mutations in RPGR exon ORF15. *Am J Hum Genet.* 2002;70:1049-1053.
  40. Burns SA, Chang He J, Delori FC. Do the cones see light scattered from the deeper layers? *Vision Science and Its Applications: Technical Digest.* Washington, DC: OSA; 1997:94-97.
  41. Delori FC, Fleckner MR, Goger DG, Weiter JJ, Dorey CK. Autofluorescence distribution associated with drusen in age-related macular degeneration. *Invest Ophthalmol Vis Sci.* 2000;41:496-504.
  42. Robson AG, Egan CA, Luong VA, et al. Comparison of fundus autofluorescence with photopic and scotopic fine-matrix mapping in patients with retinitis pigmentosa and normal visual acuity. *Invest Ophthalmol Vis Sci.* 2004;45:4119-4125.
  43. Scholl HP, Chong NH, Robson AG, et al. Fundus autofluorescence in patients with Leber congenital amaurosis. *Invest Ophthalmol Vis Sci.* 2004;45:2747-2752.
  44. Jarc-Vidmar M, Kraut A, Hawlina M. Fundus autofluorescence imaging in Best's vitelliform dystrophy. *Klin Monatsbl Augenheilkd.* 2003;220:861-867.
  45. Lois N, Halfyard AS, Bird AC, Holder GE, Fitzke FW. Fundus autofluorescence in Stargardt macular dystrophy-fundus flavimaculatus. *Am J Ophthalmol.* 2004;138:55-63.
  46. Organisciak DT, Darrow RM, Barsalou L, Kutty RK, Wiggert B. Susceptibility to retinal light damage in transgenic rats with rhodopsin mutations. *Invest Ophthalmol Vis Sci.* 2003;44:486-492.
  47. Cideciyan AV, Jacobson SG, Aleman TS, et al. In vivo dynamics of retinal injury and repair in the rhodopsin mutant dog model of human retinitis pigmentosa. *Proc Natl Acad Sci USA.* 2005;102:5233-5238.
  48. Schutt F, Davies S, Kopitz J, Holz FG, Boulton ME. Photodamage to human RPE cells by A2-E, a retinoid component of lipofuscin. *Invest Ophthalmol Vis Sci.* 2000;41:2303-2308.